Article

Structure

Structure-Function Relationship of the Bik1-Bim1 Complex

Graphical Abstract

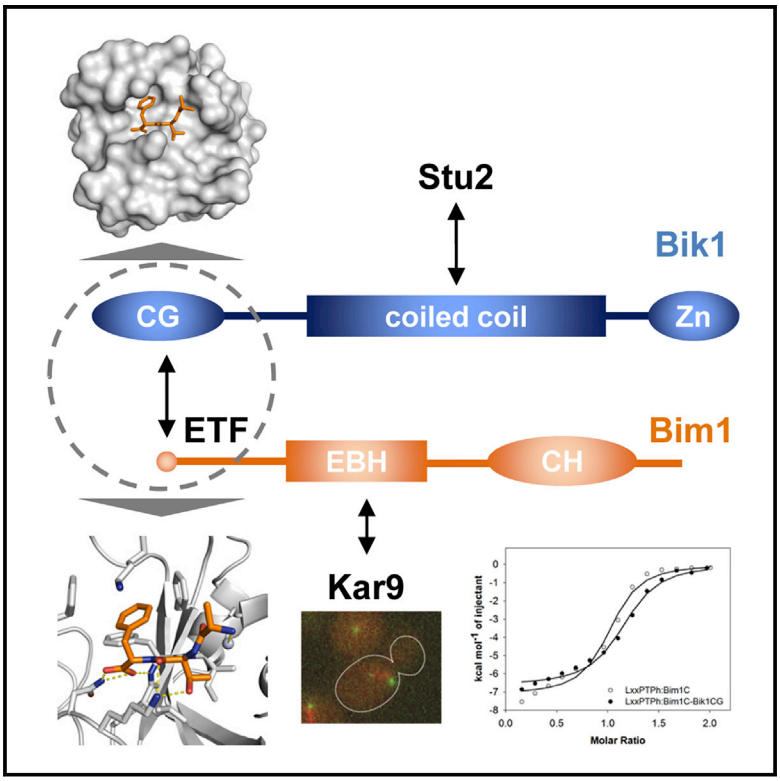

Highlights

- The CAP-Gly domain of Bik1 is a C-terminal phenylalanine recognition domain
- The Bik1-Bim1 complex interacts with the EB1-binding motifs SxIP and LxxPTPh
- Perturbation of Bik1-Bim1 affects Bik1 localization and astral microtubule length
- The Bik1/CLIP-170-Bim1/EB1 module is evolutionarily flexible

Authors

Marcel M. Stangier, Anil Kumar, Xiuzhen Chen, Ana-Maria Farcas, Yves Barral, Michel O. Steinmetz

Correspondence

michel.steinmetz@psi.ch

In Brief

Stangier et al. show that the CAP-Gly domain of Bik1 is a C-terminal phenylalanine recognition domain. Bik1-Bim1 forms ternary complexes with the EB1-binding motifs SxIP and LxxPTPh. The results provide insight into the role of the Bik1-Bim1 interaction in cell division, and demonstrate that the Bik1/CLIP-170-Bim1/EB1 module is evolutionarily flexible.

Stangier et al., 2018, Structure *26*, 607–618
April 3, 2018 © 2018 Elsevier Ltd.
https://doi.org/10.1016/j.str.2018.03.003

CellPress

Structure
Article

Structure-Function Relationship of the Bik1-Bim1 Complex

Marcel M. Stangier,[1] Anil Kumar,[1,4] Xiuzhen Chen,[2,4] Ana-Maria Farcas,[2,4] Yves Barral,[2] and Michel O. Steinmetz[1,3,5,*]
[1]Laboratory of Biomolecular Research, Division of Biology and Chemistry, Paul Scherrer Institut, 5232 Villigen PSI, Switzerland
[2]Institute of Biochemistry, ETH Zürich, 8049 Zürich, Switzerland
[3]University of Basel, Biozentrum, 4056 Basel, Switzerland
[4]These authors contributed equally
[5]Lead Contact
*Correspondence: michel.steinmetz@psi.ch
https://doi.org/10.1016/j.str.2018.03.003

SUMMARY

In budding yeast, the microtubule plus-end tracking proteins Bik1 (CLIP-170) and Bim1 (EB1) form a complex that interacts with partners involved in spindle positioning, including Stu2 and Kar9. Here, we show that the CAP-Gly and coiled-coil domains of Bik1 interact with the C-terminal ETF peptide of Bim1 and the C-terminal tail region of Stu2, respectively. The crystal structures of the CAP-Gly domain of Bik1 (Bik1CG) alone and in complex with an ETF peptide revealed unique, functionally relevant CAP-Gly elements, establishing Bik1CG as a specific C-terminal phenylalanine recognition domain. Unlike the mammalian CLIP-170-EB1 complex, Bik1-Bim1 forms ternary complexes with the EB1-binding motifs SxIP and LxxPTPh, which are present in diverse proteins, including Kar9. Perturbation of the Bik1-Bim1 interaction *in vivo* affected Bik1 localization and astral microtubule length. Our results provide insight into the role of the Bik1-Bim1 interaction for cell division, and demonstrate that the CLIP-170-EB1 module is evolutionarily flexible.

INTRODUCTION

In eukaryotic cells, various proteins localize to the plus-ends of microtubules where they regulate microtubule dynamics and attachment of microtubule ends to subcellular structures (reviewed in Howard and Hyman, 2003; Akhmanova and Steinmetz, 2015). As such, these microtubule plus-end tracking proteins (+TIPs) participate in key cellular processes, including cell division, cell motility, and intracellular trafficking. One key attribute of +TIPs is their ability to form complex and dynamic interaction networks. A detailed molecular understanding of these networks is crucial for deciphering how they support the large variety of microtubule-based processes and for rationally perturbing their architectures and functions.

Yeast is an excellent system to investigate the structure-function relationship of +TIP networks, as they are simpler than that of metazoans. In the yeast cytoplasm, +TIPs are implicated in two prominent pathways that align the mitotic spindle with the division axis of the cell, and are thus crucial for cell division: the pre-anaphase "Kar9 pathway," which involves the microtubule plus-end-F-actin crosslinking protein Kar9, and the anaphase "dynein pathway," which is supported by the microtubule minus-end directed motor protein dynein (Miller and Rose 1998; reviewed in Miller et al., 2006). Bik1 (ortholog of CLIP-170) is a crucial +TIP that acts together with proteins of both pathways (reviewed in Miller et al., 2006). It interacts directly and indirectly with microtubules (Badin-Larçon et al., 2004), with the GTP-cap-binding protein Bim1 (ortholog of the end binding [EB] protein EB1; Blake-Hodek et al., 2010), Stu2 (ortholog of the microtubule polymerase XMAP215/ch-TOG; Podolski et al., 2014), and Kar9 (Moore et al., 2006), and is thus a central player in +TIP networks. However, how these diverse interactions are orchestrated, whether they are simultaneous or mutually exclusive, and how they contribute to Bik1 function is poorly understood.

In this study, we assessed the structural basis and function of Bik1-Bim1-mediated interactions. Bik1 consists of an N-terminal cytoskeleton-associated protein glycine-rich (CAP-Gly) domain, which is followed by a positively charged unstructured region, a coiled-coil domain, and a zinc finger domain at its C terminus (Figure 1A; reviewed in Miller et al., 2006). The CAP-Gly domains of CLIP-170 and p150glued interact with the C-terminal EEY motif of EBs, whereby the terminal tyrosine residue is essential for binding (Weisbrich et al., 2007). However, this tyrosine can be substituted by a phenylalanine residue without compromising the binding strength toward the CAP-Gly domains of both CLIP-170 and p150glued (Weisbrich et al., 2007; Mishima et al., 2007). Notably, C-terminal EEY/F motifs that are targeted by CAP-Gly domains are also present in α-tubulin, CLIP-170, and SLAIN2 (reviewed in Slep, 2010; Steinmetz and Akhmanova, 2008). Based on these observations, CAP-Gly domains were defined as EEY/F motif recognition domains (reviewed in Steinmetz and Akhmanova, 2008). Besides CAP-Gly domains, EBs also interacts with linear SxIP and LxxPTPh motifs present in many +TIPs, including Kar9 (Honnappa et al., 2009; Kumar et al., 2017). Notably, binding of mammalian EB1 to both CAP-Gly and to SxIP are reciprocally exclusive, due to competition between these two elements for adjacent binding sites (Duellberg et al., 2014). The evolutionary flexibility of these modules, however, is unknown.

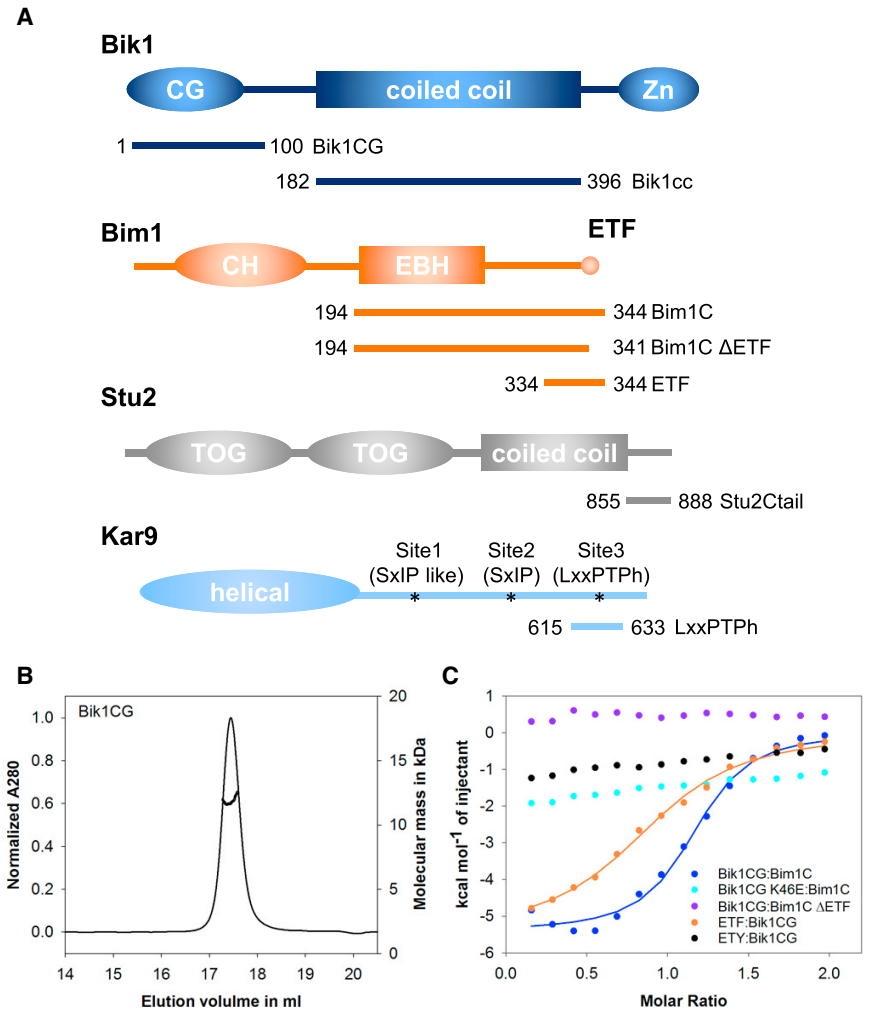

Figure 1. Schematic Representations of Proteins and Constructs Used in this Study

(A) Respective protein fragments are labeled and indicated by lines and residue boundaries. Asterisks in Kar9 indicate the positions of the Bim1-interacting site 1, site 2, and site 3 (Manatschal et al., 2016). CG, CAP-Gly; Zn, zinc finger; CH, calponin homology; EBH, end binding (EB) homology; TOG, tumor overexpressed gene.

(B) SEC-MALS experiment of Bik1CG. The UV absorption at 280 nm and the molecular masses across the peak determined by MALS are plotted.

(C) ITC experiments for Bik1CG:Bim1C (blue closed circles), Bik1CG K46E:Bim1C (cyan closed circles), Bik1CG:Bim1C ΔETF (purple closed circles), ETF:Bik1CG (orange closed circles), and ETY:Bik1CG (black closed circles). Solid lines are the fits that were obtained by using the monomeric concentrations of the proteins.

See also Table S1 and Figure S1.

Here, using biophysical methods in combination with mutagenesis, we found that the CAP-Gly domain of Bik1 (Bik1CG) binds to the C-terminal ETF peptide of Bim1 in the low-micromolar range. In contrast to the CAP-Gly domains of CLIP-170 and p150glued, the Bik1CG showed strict specificity, preventing it from binding to Bim1 when the terminal phenylalanine was substituted by a tyrosine residue. Furthermore, unlike CLIP-170-EB1 and p150glued-EB1, the Bik1-Bim1 complex allows SxIP and LxxPTPh motifs to bind. The crystal structures of the Bik1CG alone and in complex with an ETF peptide identifies essential residues for the formation of the Bik1-Bim1 complex in both Bik1 and Bim1. We used this structural information to assess the role of the Bik1-Bim1 interaction in controlling Bik1 localization, astral microtubule length, and spindle positioning.

RESULTS

Biophysical Characterization of the Bik1-Bim1 Interaction

To quantitatively analyze the interaction of the Bik1CG with the C terminus of Bim1 (Bim1C) (Figures 1A and S1) (Blake-Hodek et al., 2010), we purified these recombinant protein fragments from bacteria. Bim1C forms dimers in solution (Blake-Hodek et al., 2010; Hüls et al., 2012; Manatschal et al., 2016). As shown in Figure 1B, size-exclusion chromatography followed by multi-angle light scattering (SEC-MALS) revealed a molecular mass for Bik1CG of 11.6 kDa, consistent with the presence of a monomer (calculated molecular mass of the Bik1CG monomer construct: 11.2 kDa). Complex formation between Bik1CG monomers and Bim1C dimers was monitored by isothermal titration calorimetry (ITC). The data presented in Figure 1C demonstrate that two Bik1CG monomers bind one Bim1C dimer with an equilibrium dissociation constant (K_D) of 1.2 ± 0.3 μM.

Bim1C contains the EB-homology (EBH) domain and a C-terminal disordered tail region that terminates with an EEY/F motif (ETF in the case of Bim1C; Figure 1A). To test the exact interaction mode of Bik1CG with Bim1C, we performed ITC experiments with a Bim1C version that lacks the last three C-terminal residues (Bim1C ΔETF) and with a Bim1-derived peptide containing the ETF motif. As shown in Figure 1C, one Bik1CG monomer bound one ETF peptide with a K_D of 5.6 ± 0.8 μM. In contrast, no interaction was observed between Bik1CG and Bim1C ΔETF (Figure 1C). Thus, the interaction between Bik1CG and Bim1C is primarily mediated by the ETF motif of Bim1.

Crystal Structures of Bik1CG and the Bik1CG-Bim1C Complex

To obtain a detailed insight into how Bik1 and Bim1 interact with each other, we solved the structure of Bik1CG alone and in complex with the C-terminal ETF peptide of Bim1C (denoted Bik1CG-ETF) to 1.9 and 1.8 Å resolution, respectively (Table 1). As shown in Figure 2A, the globular apo Bik1CG structure contains a highly twisted, five-stranded antiparallel β sheet that is flanked by a small β hairpin on its convex side, structural features

Table 1. X-Ray Data Collection and Refinement Statistics

	Bik1CG	Bik1CG-ETF
Data collection[a]		
Space group	$P4_1\,2_1\,2$	$P4_1\,2_1\,2$
Cell dimension		
a, b, c (Å)	53.7, 53.7, 61.4	53.6, 53.6, 62.0
α, β, γ (°)	90, 90, 90	90, 90, 90
Resolution (Å)[b]	40.4–1.88 (1.95–1.88)	40.55–1.8 (1.87–1.8)
R_{meas} (%)	10.0 (97.8)	28.7 (438.0)
R_{pim} (%)	2.0 (19.9)	5.7 (88.5)
CC½[c]	99.9 (85.9)	99.8 (38.8)
I/σI	28.2 (3.4)	13.2 (0.9)
Completeness (%)	99.8 (98.4)	100 (99.8)
Redundancy	25.0 (22.5)	25.3 (24.1)
Refinement		
Resolution (Å)	40.4–1.88	40.54–1.8
No. of unique reflections	7,731	8,808
R_{work}/R_{free} (%)	16.7/19.7	18.5/22.9
Average B factors	34.3	33.6
RMSD from ideality		
Bond length (Å)	0.02	0.02
Bond angles (°)	1.84	1.68
Ramachandran statistics (%)[d]		
Favored regions	97.6	97.6
Allowed regions	2.4	2.4
Outliers	0	0

[a]Highest-resolution shell statistics are in parentheses. RMSD, root-mean-square deviation.
[b]The resolution cutoff was selected based on I/σI and CC½ according to Karplus and Diederichs (2012).
[c]CC½ is the percentage of correlation between intensities from random half-datasets.
[d]As defined by MolProbity (Davis et al., 2004).

that are characteristic of the CAP-Gly fold (reviewed in Steinmetz and Akhmanova, 2008). The structure is complemented by two unique α helices that pack against the concave side of the central β sheet, secondary structure elements that have not been observed in any CAP-Gly structure solved until now. Most of the glycine residues that are highly conserved across CAP-Gly domains are involved in shaping the loop regions of the Bik1CG structure. Furthermore, a unique cluster of conserved hydrophobic residues that pack against each other forms a solvent-exposed cavity bordered by the distinctive GKNDG sequence motif (Figure 2B); this cavity binds C-terminal EEY/F motifs (reviewed in Steinmetz and Akhmanova, 2008).

Superimposition of Bik1CG with the first CAP-Gly domain of CLIP-170 (CLIP170CG1) (Weisbrich et al., 2007) and that of p150glued (p150CG) (Honnappa et al., 2006) revealed that, with the exception of helices H1 and H2, which are unique to Bik1CG, the domains are very similar (root-mean-square deviation $[RMSD]_{Bik1CG\text{-}CLIP170CG1}$: 0.7 Å over 43 Cα atoms; $RMSD_{Bik1CG\text{-}p150CG}$: 0.8 Å over 45 Cα atoms). However, inspection of the hydrophobic cavities of Bik1CG, CLIP170CG, and p150glued revealed a prominent difference in the β2-β3 loop that adopts a more "open" conformation in the case of Bik1CG (Figure 2C). This difference is most likely due to Thr30 of Bik1CG, which adopts an "outward," exposed conformation. In contrast, the corresponding residue in CLIP170CG and p150CG is occupied by a phenylalanine that assumes an "inward" conformation and whose side chain packs against surrounding hydrophobic core CAP-Gly residues (Figure 2C). As a consequence, the hydrophobic cavities of CLIP170CG and p150CG, which are essentially identical, is shallower than that of Bik1CG. However, the open conformation of the β2-β3 loop as well as the N- and C-terminal flanking helices are very likely to be conserved in budding yeast Bik1 proteins (Figure S2), suggesting functional conservation across budding yeast species. Collectively, these observations indicate that the hydrophobic cavity of the Bik1CG is shaped distinctly from that of its metazoan ortholog CLIP-170.

Whereas CLIP170CG1 binds primarily the C-terminal EEY peptide of EB1, p150CG simultaneously binds both EEY and the EBH domain (Weisbrich et al., 2007; Honnappa et al., 2006; Mishima et al., 2007; Bjelić et al., 2012). The determinant discriminating between the single and bipartite binding mode is primarily a residue in the β2-β3 loop of the CAP-Gly domain, Ala49 and Glu79 of p150CG and CLIP170CG1, respectively (Figure 2E). In the case of p150CG, the Ala49 side chain packs against the hydrophobic groove of the EBH domain of EB1, while, in the case of CLIP170CG1, the Glu79 side chain is expected to inhibit such an interaction (Honnappa et al., 2006; Bjelić et al., 2012). In Bik1CG, the equivalent β2-β3 loop residue position is occupied by a proline (Pro27). To understand why Bik1CG does not interact with Bim1C-ΔETF in solution (Figure 1C), we superimposed the Bik1CG structure onto that of p150CG in complex with the C-terminal domain of EB1 (Honnappa et al., 2006; Bjelić et al., 2012). As illustrated in Figure 2D, this analysis reveals that Pro27 of Bik1CG substitutes well for the alanine in p150CG, thus making an interaction of the β2-β3 loop of Bik1CG with the EBH domain of Bim1 in principle possible. However, we observed that the unique N-terminal helix H1 of Bik1CG seriously clashes into the four-helix bundle of the EBH domain of EB1 (Figure 2D). This observation explains why Bik1CG does not interact with Bim1C ΔETF.

Next, we inspected the structure of the Bik1CG-ETF complex. Superimposition of Bik1CG and Bik1CG-ETF revealed that, besides an outward movement of the side chain of Lys31, which is needed to accommodate binding of the ETF peptide to Bik1CG, no additional conformational changes are observed ($RMSD_{Bik1CG\text{-}Bik1CG\text{-}ETF}$: 0.1 Å over 79 Cα atoms). As expected, the ETF peptide is bound to the hydrophobic cavity of Bik1CG, which is bordered by the highly conserved GKNDG motif (Figure 3A). Well-defined electron density is seen for the TF dipeptide and for the main chain of the glutamate residue of ETF. The side chain of Phe344 of the ETF peptide is deeply inserted into the hydrophobic cavity of Bik1CG, which is shaped by the side chains of Val28, Lys31, Phe35, Phe51, and Phe67 (Figure 3B). Three prominent hydrogen-bonding interactions are established between the carboxylate and main chain amide group of Phe344 of ETF and the side chain and main chain of Asn47 (the asparagine of the GKNDG motif) and Ph67 of Bik1CG (Figure 3C). Three additional hydrogen bonds are formed between the main chain of Phe344 and side chain of Thr343 of ETF and the side

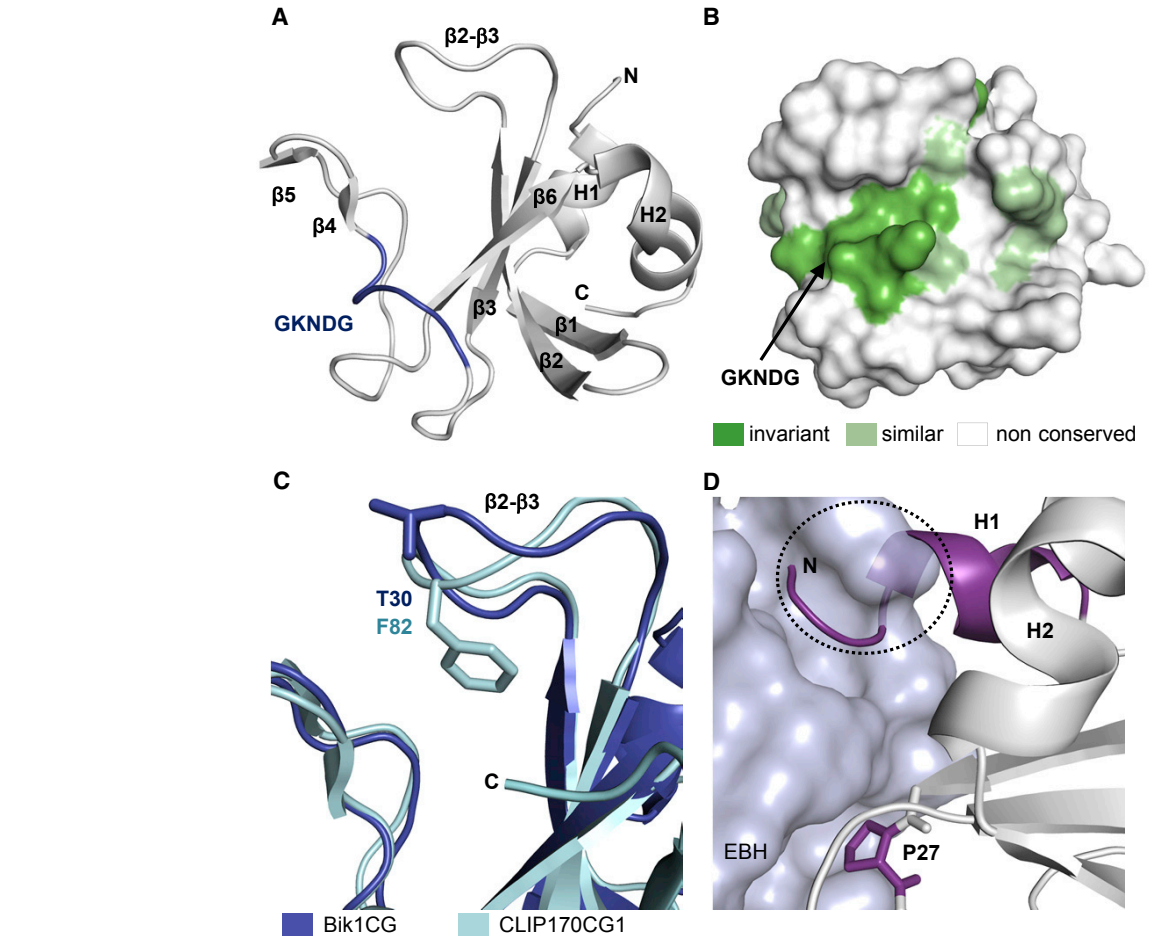

Figure 2. Crystal Structure of the Bik1CG

(A) Overall view of the Bik1CG structure in cartoon representation with the highly conserved GKNDG motif highlighted in light blue. Secondary structure elements are indicated. In contrast to the CAP-Gly domains of higher eukaryotes, Bik1CG possesses two additional helices (H1 and H2); see also (E).

(B) Surface representation of the Bik1CG structure with conserved residues between Bik1CG, CLIP170CG1, and p150CG highlighted in green.

(C) Superimposition of Bik1CG (dark blue) with CLIP170CG1 (cyan) (PDB: 2E3I) highlighting structural differences in the hydrophobic cavity of the two CAP-Gly domains.

(D) Close-up view of the superimposition of Bik1CG (cartoon representation) with p150CG (not shown for simplicity) in complex with the EBH domain of EB1 (surface representation; PDB: 2HKQ). The clash caused by the N-terminal helix H1 (shown in maroon) of Bik1CG with the EBH domain is highlighted with a dashed black circle. Pro27 of Bik1CG is shown in blue sticks representation.

(E) Sequence alignment of the CAP-Gly domains of Bik1, CLIP-170 (CG1), and p150glued. The characteristic glycine residues and GKNDG motif of CAP-Gly domains are indicated in green and with a black horizontal bar on top of the alignment, respectively. The position of the β2-β3 loop residue that in the case of p150CG interacts with the EBH domain of EB1 (Ala49; Honnappa et al., 2006) is highlighted with an asterisk, and the corresponding residues are shown in bold and purple. Key residues of the exposed hydrophobic cavity of CAP-Gly, which are discussed in the text, are shown in bold and dark blue. Note that helices H1 and H2 (indicated in light blue) are only found in Bik1.

See also Figure S2.

chain of Lys46 of Bik1CG (the lysine of the GKNDG motif), and through a water molecule between the main chain of Glu342 of ETF and the main chain of Gln69 and the side chain of Lys72 of Bik1CG (Figure 3C). The apparent importance of Lys46 of the GKNDG motif of Bik1CG for Bim1C binding was tested by mutagenesis. As documented in Figure 1C, mutating this residue to glutamate (Bik1CG K46E) is sufficient to abrogate binding of the mutant domain to Bim1C in ITC experiments.

Comparison of the Bik1CG-ETF binding mode with those seen in the complex structures formed between p150CG and the

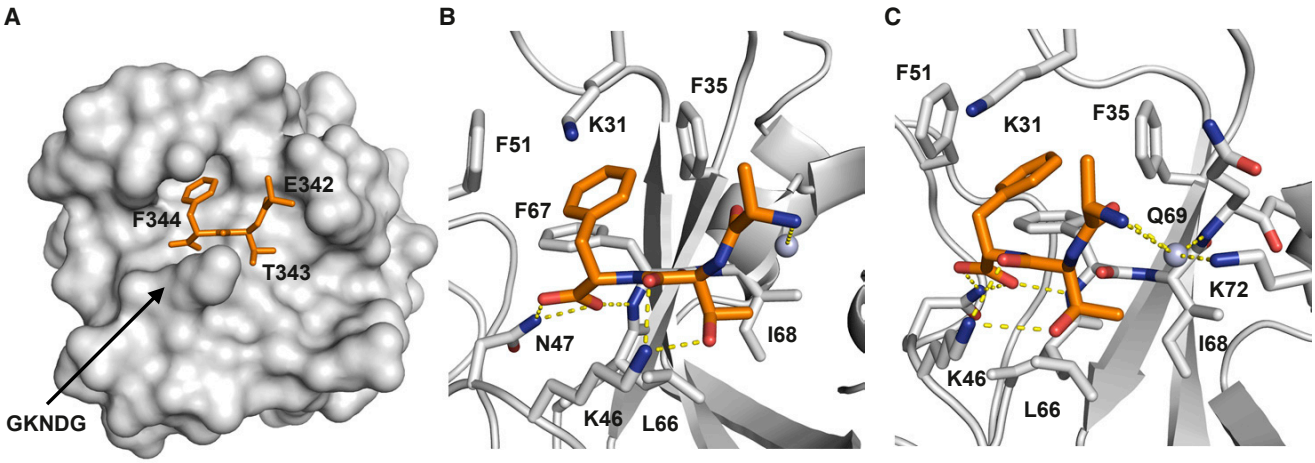

Figure 3. Crystal Structure of the Bik1CG-ETF Complex

(A) Overall view of the heterodimeric complex formed between Bik1CG (gray surface representation) and the ETF peptide of Bim1 (orange sticks representation). (B and C) Two close-up views of the complex formed between Bik1CG (gray) and the ETF peptide of Bim1 (orange) 90° apart. Interacting residues are shown in sticks representation.

C-terminal EEY peptide of EB1 (Honnappa et al., 2006; Bjelić et al., 2012), between p150CG and the C-terminal ETF peptide of CLIP-170 (Weisbrich et al., 2007), and between CLIP170CG1 and the C-terminal GCY peptide of SLAIN2 (van der Vaart et al., 2011), revealed that the CAP-Gly-EEY/F motif binding modes are overall similar for all four complex structures (Figures 4A and B). However, and interestingly, we noted that the terminal Phe344 residue of the ETF peptide of Bim1C is much deeper inserted into the binding pocket compared with its aromatic residue counterparts of the other CAP-Gly-EEY/F motif complex structures. This deeper insertion of Phe344 is most likely achieved due to the open conformation of the β2-β3 loop, which widens the cavity. In addition, the side chains of Lys31 and Phe51 of Bik1CG, which are substituted by Ala and Val, respectively, in both p150CG and CLIP170CG1, allow for a more extensive packing with the C-terminal phenylalanine residue of the Bim1 ETF peptide (Figure 4C).

Modeling of the binding mode of the Bim1 ETF peptide in the context of CLIP170CG1 or p150CG revealed that the terminal phenylalanine side chain of ETF would clash into the phenylalanine residue forming the floor of the cavity (Phe52 in the case of p150CG; Figure 4C) due to the more closed conformation adopted by the β2-β3 loop of both these CAP-Gly domains (Figure 4D). Inversely, computational replacement of the phenylalanine residue of ETF in the Bik1CG-ETF complex structure by a tyrosine indicates that its polar side chain OH group would be placed in a strongly hydrophobic environment and would probably even clash into the protein domain (not shown). To test this hypothesis, we performed ITC experiments with a mutant C-terminal Bim1C ETF peptide variant in which the terminal phenylalanine was replaced by a tyrosine (ETY peptide). As shown in Figure 1C, binding of the ETY peptide to Bik1CG was essentially abrogated compared with the wild-type ETF peptide.

Taken together, these results reveal the structural basis of the Bik1-Bim1 interaction and establish the Bik1CG as a C-terminal phenylalanine recognition domain. Notably, the unique phenylalanine-binding pocket of Bik1 CAP-Gly enables the domain to achieve a 1–2 orders of magnitude higher affinity toward C-terminal EEF motifs compared with the CAP-Gly domains of CLIP-170 or p150glued, which target both EEY and EEF motifs (Weisbrich et al., 2007; Honnappa et al., 2006; Bjelić et al., 2012).

Interaction of the Bik1-Bim1 Complex with +TIP Partners

As mentioned in the Introduction, Bik1 has the capacity to interact directly or indirectly with additional +TIP partners, including Kar9 and Stu2 (Figure S1). For instance, the C-terminal unstructured domain of Kar9 interacts with Bim1C via SxIP and LxxPTPh motifs (Figure 1A), which bind to the EBH domain of Bim1C (Manatschal et al., 2016; Kumar et al., 2017). This observation suggests that Kar9 binds mainly indirectly to Bik1 via Bim1. To test this hypothesis, we performed ITC experiments with the Bik1CG-Bim1C complex and SxIP and LxxPTPh peptides. As shown in Figures 5A and B, and summarized in Table S1, the Bik1CG-Bim1C complex binds SxIP or LxxPTPh peptides with K_D values of 13 ± 0.6 and 2.7 ± 0.5 μM, respectively, values that are close to those obtained with Bim1C alone. We also assessed the affinity of the Bim1C-SxIP complex toward Bik1CG, and obtained a very similar K_D as for the Bim1C-Bik1CG interaction (Table S1). Collectively, these results suggest that Kar9 can indeed bind Bik1 indirectly via Bim1.

Next, we tested whether Stu2 binds Bik1 directly or indirectly. Two-hybrid, coimmunoprecipitation, and *in vitro* binding assays suggested an interaction between the predicted coiled-coil domain of Bik1 (Bik1cc) and the C-terminal disordered tail region of Stu2 (Stu2Ctail) (Wolyniak et al., 2006). To reconstitute a putative Bik1cc-Stu2Ctail complex, we purified the corresponding recombinant protein fragments from bacteria. The secondary structure and stability of Bik1cc were assessed by circular dichroism (CD) spectroscopy. As shown in Figure 6A, the far-UV CD spectrum of the protein recorded at 5°C displays minima at 208 and 222 nm, which is characteristic of α-helical

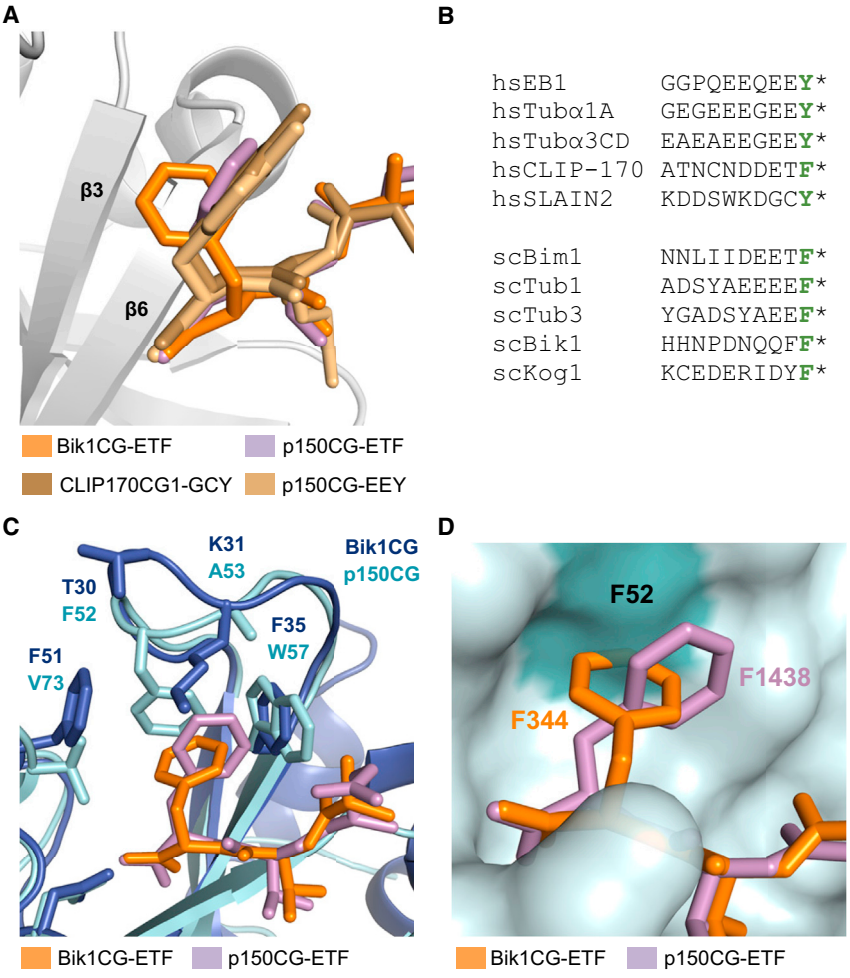

Figure 4. Analysis of the Bik1CG-ETF Complex

(A) Superimposition of Bik1CG-ETF compared with those complex structures formed between CLIP170CG1 and the C-terminal GCY peptide of SLAIN2 (CLIP170CG1-GCY) (PDB: 3RDV), between p150CG and the C-terminal ETF peptide of CLIP-170 (p150CG-ETF) (PDB: 3E2U), and between p150CG and the C-terminal EEY peptide of EB1 (p150CG-EEY) (PDB: 2HL3). For simplicity, only the structure of Bik1CG is shown in cartoon representation. The different peptide motifs are shown in sticks representation.

(B) Sequence alignment of human proteins containing C-terminal EEY motifs and yeast proteins containing C-terminal EEF motifs.

(C) Superimposition of the Bik1CG-ETF (dark blue) and p150CG-ETF (cyan) complex structures (cartoon representation). Interacting residues are shown in sticks representation.

(D) Close-up view of (C) with p150CG in semi-transparent surface representation.

proteins. Upon heating and recording of the CD signal at 222 nm, a cooperative thermal unfolding profile with a midpoint of the transition at 37°C was obtained for Bik1cc (Figure 6B). The oligomerization state of Bik1cc in solution was assessed by SEC-MALS, which yielded a molecular mass of 50.6 kDa, consistent with the formation of a dimer (calculated molecular mass of the Bik1cc monomer: 25.5 kDa; Figure 6C). These results suggest that Bik1cc folds into a two-stranded coiled-coil structure.

The interaction between Bik1cc and Stu2Ctail was subsequently assessed by ITC. The data shown in Figure 6D revealed that one Stu2Ctail peptide binds one Bik1cc dimer with a K_D of 0.6 ± 0.1 μM. Stu2Ctail has also been reported to interact with Bim1C (Wolyniak et al., 2006); however, we were not able to detect such an interaction in ITC experiments (Figure 5D). +TIP peptide regions that bind to the C-terminal domain of EB proteins typically contain SxIP or LxxPTPh motifs (Honnappa et al., 2009; Kumar et al., 2017). No such motifs were found in the Stu2Ctail sequence, explaining the inability of this Stu2 region to interact with Bim1C (Wolyniak et al., 2006). Taken together, these results establish a molecular and quantitative basis for understanding the indirect interaction between Bik1 and Kar9, the direct interaction between Bik1 and Stu2, and the indirect interaction between Stu2 and Bim1.

Role of Bik1 CAP-Gly Domain-Mediated Interactions *In Vivo*

Although it has been shown that the accumulation of Bik1 on microtubule plus-ends relies on both Bim1 and α-tubulin (Caudron et al., 2008), it is unknown whether this dependency stems from the direct interaction between the Bik1 CAP-Gly domain and the C-terminal EEF motifs of Bim1 and α-tubulin. To dissect the function of the Bik1-Bim1 complex and other Bik1 CAP-Gly domain-mediated interactions, we created yeast strains that specifically lose the Bik1-Bim1 interaction by deleting the C-terminal ETF peptide of Bim1 (Bim1 ΔETF) or strains bearing the K46E point mutation in the Bik1 CAP-Gly domain (Bik1 K46E), which fail to interact with EEY/F motifs. Interestingly, the Bim1 ΔETF cells did not show any growth defect on YPD plates, while Bik1 K46E mutant cells exhibited a severe growth defect, similar to the *bik1Δ* mutant cells (Figure 7A). This result suggests that the interaction of the Bik1CG with EEF is essential for Bik1 function. Furthermore, binding to the ETF peptide of Bim1 is not sufficient to express the full function of the CAP-Gly domain of Bik1.

We next assessed the impact of these mutations on the recruitment of Bik1-3xGFP to astral microtubule plus-ends. As shown in Figures 7B–7D, the disruption of Bik1-Bim1 interaction either by deleting BIM1 or its C-terminal ETF peptide, reduced the accumulation of Bik1-3xGFP on plus-ends by more than 35%. Interestingly, we noticed that a substantial amount of Bik1-3xGFP binds microtubule lattices upon loss of the Bik1-Bim1 interaction. This dramatic change is quantified by line scan analyses of Bik1-3xGFP fluorescence intensity along microtubules from plus-ends toward the spindle pole bodies (SPBs) (Figures 7B–7D). Furthermore, concomitant disruption of Bik1-Bim1 and Bik1-α-tubulin interactions by

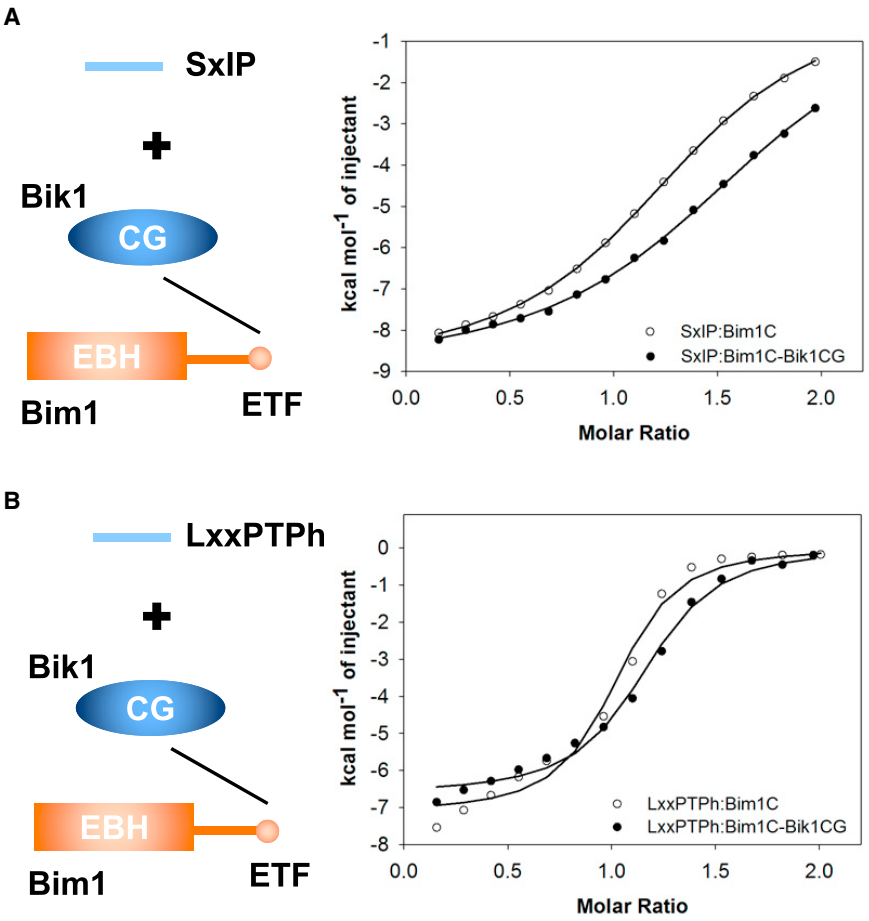

Figure 5. Ternary Complex Formation of Bik1-Bim1 with SxIP or LxxPTP Motifs

(A) ITC experiment for SxIP:Bim1C (open circles) and SxIP:Bim1C-Bik1CG (closed circles). Solid lines are the fits that were obtained by using the monomeric concentrations of the proteins.

(B) ITC experiments for LxxPTPh:Bim1C (open circles) and LxxPTPh:Bim1C-Bik1CG (closed circles).

Solid lines are the fits that were obtained by using the monomeric concentrations of the proteins and peptides.

See also Table S1 and Figure S1.

introducing the K46E substitution in the Bik1CG drastically reduced the Bik1 K46E-3xGFP intensity both at the plus-ends and along astral microtubules. Only around 17.7% of the Bik1 K46E-3xGFP mutant metaphase cells (77 out of 436) demonstrated detectable signal on astral microtubule plus-ends. In those cells, the Bik1 K46E-3xGFP focus on astral microtubule plus-ends was very faint. These observations establish two points. First, Bik1 interacts with microtubules essentially through binding to EEF motifs, i.e., to the C-terminal tails of Bim1 and α-tubulin. Second, somehow Bim1 helps displacing Bik1 from the microtubule shaft.

Next, we investigated the consequences of abrogating the Bik1-Bim1 interaction on microtubule dynamics in metaphase. Using Bik1-3xGFP and Spc72-GFP as microtubule plus-end and minus-end markers, respectively, we measured the maximum 3D length and lifetime of individual astral microtubules over an image acquisition window of 85.6 s. Deletion of BIM1 increased the maximum astral microtubule length from 2.08 ± 0.62 to 3.54 ± 0.76 μm (mean ± SD). The lifetimes of astral microtubules were also increased (Figures 7E and 7F). These observations support the idea of EB proteins being microtubule-destabilization factors by accelerating GTP hydrolysis in the GTP cap of growing microtubules (Maurer et al., 2014). Importantly, the loss of the Bik1-Bim1 interaction in Bim1 ΔETF cells increased the size of astral microtubules to 2.62 ± 0.72 μm (mean ± SD) (Figures 7E and 7F). Knowing that Bik1 functions as a microtubule-stabilizing factor *in vivo* (Carvalho et al., 2004; Caudron et al., 2008), together with the fact that the Bik1 amount is reduced on astral microtubule plus-ends in Bim1 ΔETF cells (Figures 7C and 7D), we reasoned that Bik1 could promote the microtubule-destabilizing activity of Bim1. Unfortunately, the very low intensity of Bik1 K46E-3xGFP on plus-ends prevented us from quantifying astral microtubule behavior in these cells. Together, these data demonstrate that the interaction of Bik1 with Bim1 and α-tubulin, mediated by the Bik1 CAP-Gly domain, ensures the accumulation of Bik1 on the plus-end of microtubules, while displacing it from the microtubule lattice. They further reveal that the Bik1-Bim1 interaction promotes astral microtubule destabilization.

To test whether the Bik1-Bim1 interaction contributes to spindle positioning during metaphase, we introduced the Bik1 K46E and Bim1 ΔETF mutations into strains expressing the Tub1 protein tagged with CFP to visualize the mitotic spindle, where the Kar9 protein was tagged with 3xsfGFP To assess the function of Kar9 during metaphase, we measured the relative spindle positioning to the mother-bud neck and the alignment along the mother-bud axis in wild-type cells. We then compared these results across strains bearing the *bik1 K46E*, the *bim1 ΔETF*, and the *kar9Δ* genotypes. As shown in Figures 7G and 7H, disrupting the Bik1-Bim1 interaction by either mutating Bik1 or Bim1 did not interfere with Kar9 localization and function. On the contrary, the mutations disrupting the Bik1-Bim1 interaction caused a slight improvement of spindle positioning compared with wild-type (Figure 7I). Thus, the disruption of the Bik1-Bim1 interaction impairs the proper localization of Bik1 at microtubule plus-ends, resulting in longer microtubules, whereas there is no significant effect on Kar9 localization, Kar9 asymmetry, and spindle positioning.

DISCUSSION

Although a rudimentary understanding of the interactions mediated by the CLIP-170 family member Bik1 with protein partners is available, it is unclear whether these interactions are direct or

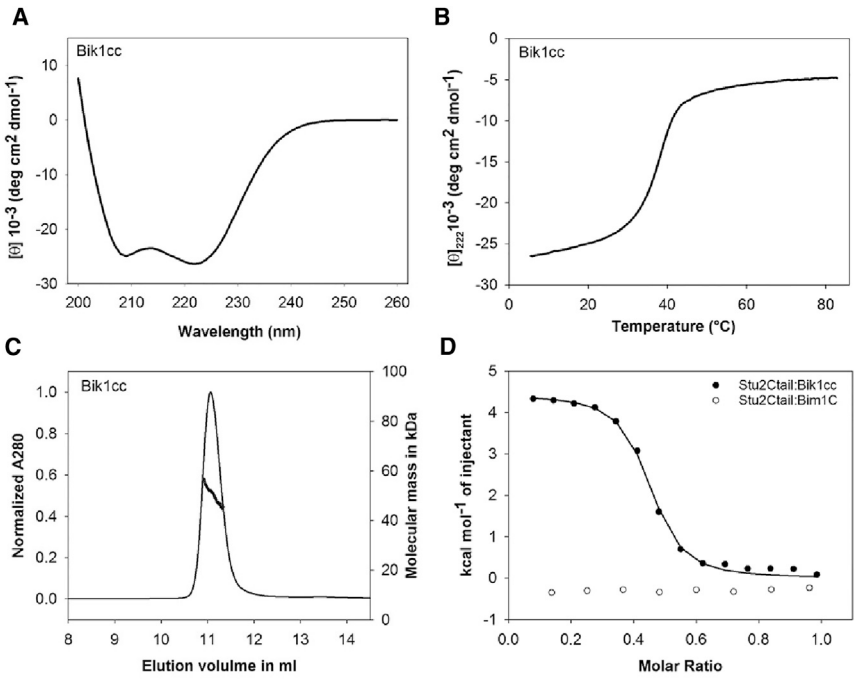

Figure 6. Biophysical Characterization of Bik1 Interactions

(A and B) CD spectrum (A) and thermal unfolding profile recorded at 222 nm (B) of Bik1cc.

(C) SEC-MALS experiment of Bik1cc. The UV absorption at 280 nm and the molecular masses across the peak determined by MALS are plotted.

(D) ITC experiments for Stu2Ctail:Bik1cc (closed circles) and Stu2Ctail:Bim1C (open circles). The solid line represents the fit that was obtained by using the monomeric concentrations of Bik1cc and Stu2Ctail.

See also Table S1 and Figure S1.

indirect. Furthermore, quantitative and structural information on Bik1-mediated complexes is largely missing. The availability of such information is, however, important to understand how Bik1 interactions contribute to its functions.

In this study, we found that the Bik1CG is a specific C-terminal phenylalanine recognition domain. Interestingly, besides Bim1 C-terminal phenylalanine residues that are targeted by the Bik1CG are also present in the budding yeast proteins α-tubulin and the TORC1 subunit Kog1/Raptor (Badin-Larçon et al., 2004; van der Vaart et al., 2017). In contrast, proteins that are targeted by the CAP-Gly domains of mammalian CLIP-170 and p150glued contain predominantly C-terminal tyrosine residues (Figure 4B). Thus, besides offering detailed structural insights into the Bik1-Bim1 complex, our results also provide a basis for understanding the Bik1-α-tubulin and Bik1-Kog1/Raptor interactions. We further found that the Bik1CG contains a unique N-terminal helix that prevents interaction with the EBH domain of EBs; CLIP-170 CAP-Gly achieves a similar effect, however, through the presence of an unfavorable residue located in the β2-β3 loop of the domain (Honnappa et al., 2006). Collectively, these observations highlight that, within the CLIP-170 protein family, the CAP-Gly domain structurally evolved along different routes to nevertheless achieve a similar binding mechanism toward proteins containing C-terminal EEY and/or EEF motifs.

We also report that the Bik1CG-ETF complex can interact with SxIP or LxxPTPh peptides. Ternary +TIP complexes are thus likely to be formed, for example, between Bim1-Bik1 and Kar9 or the yeast kinesin motor Kip2, two +TIPs that contain SxIP and/or LxxPTPh motifs and which are important for spindle alignment and proper function of the motor dynein (Roberts et al., 2014; Manatschal et al., 2016; Kumar et al., 2017). Interestingly, and in contrast to Bik1-Bim1, the CLIP-170-EB1 complex is not capable to bind SxIP peptides (Duellberg et al., 2014). This evolutionary flexibility can be explained by the significantly shorter C-terminal tail sequence of EB1 compared with Bim1 (19 compared with 67 residues, respectively), which, upon CLIP-170 CAP-Gly binding, apparently hinders access of SxIP to its EB1-binding site in the CLIP-170-EB1 complex.

In addition to the CAP-Gly domain that mediates the interaction of Bik1 with Bim1, α-tubulin and Kog1/Raptor, we found that the Bik1cc binds the C-terminal tail region of Stu2 with high affinity. The fact that Bik1 forms complexes with several protein partners through its different domains suggests that Bik1 acts as an adaptor protein that can link different activities to the same location. Although Stu2 is an autonomous +TIP (Podolski et al., 2014), the indirect interaction to Bim1 through Bik1 is likely relevant to enhance its localization to the otherwise crowded environment of the microtubule plus-end. Stu2 has also been reported to interact with Kar9 (Moore and Miller, 2007), which creates an additional indirect link between Stu2 and the Bik1-Bim1 complex. Interestingly, in fission yeast the Bim1 ortholog Mal3 is capable of directly interacting with the Stu2 paralog Dis1 via an LxxPTPh motif (Matsuo et al., 2016; Kumar et al., 2017). In higher eukaryotes, SLAIN2 forms an adaptor complex with CLIP-170 to indirectly link the Stu2 ortholog ch-TOG to EBs at growing microtubule plus-ends (van der Vaart et al., 2011). Taken together, these biophysical and structural considerations highlight the complex topology that +TIP networks can adopt at growing microtubule plus-ends, and whose connectivity and interaction strength of individual nodes can vary from one species to the other, although the involved domains and motifs belong to the same protein family.

The structure of the Bik1CG-ETF complex allowed us to rationally mutate residues with the aim to perturb the Bik1-Bim1 interaction *in vivo*. We found that deleting the ETF motif of Bim1 resulted in a reduction in Bik1 localization to microtubule plus-ends, and an increase in the amount of Bik1 decorating microtubule shafts, probably via the EEF motif of α-tubulin. The remaining tip-localized pool could be maintained through Stu2-binding, transport of Bik1 via the kinesin motor Kip2 (Carvalho et al., 2004), and through interactions

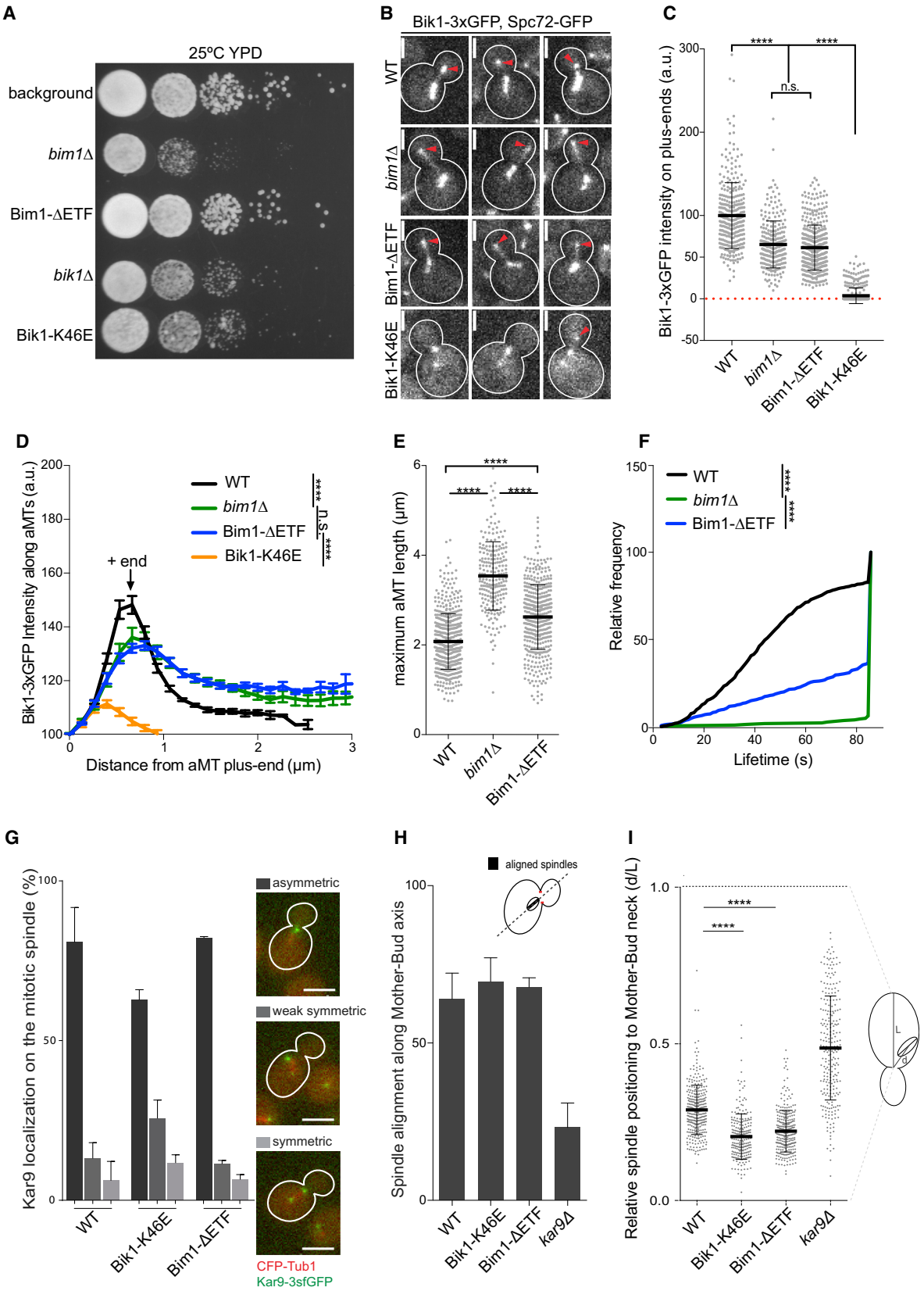

(legend on next page)

with the EEF motif of α-tubulin (Badin-Larçon et al., 2004). Thus, and as reported earlier (Caudron et al., 2008), it seems that Bik1 exhibits two partially redundant mechanisms for localizing to microtubule plus-ends. The increased levels of Bik1 on microtubule shafts suggests that somehow Bim1 helps removing Bik1 from microtubules, perhaps by competing with α-tubulin.

Interestingly, the average microtubule length was increased in a Bim1 ΔETF background, but remained still smaller than in the Bim1 delete strain. The most likely explanation for this intermediate phenotype is that, in the Bim1 delete background, many more Bim1-dependent interactions are perturbed compared with Bim1 ΔETF, thus resulting in a stronger microtubule length phenotype. The disruption of the Bik1-Bim1 interaction did not significantly perturb the asymmetric positioning of Kar9 and, accordingly, the positioning and alignment of the mitotic spindle. It has been reported that the deletion of Bik1 resulted in partial loss of Kar9 asymmetry (Moore et al., 2006). In this context, our data suggest that this Bik1-dependent Kar9 asymmetry does not rely on the Bik1-Bim1 interaction. In conclusion, our study provides detailed mechanistic and functional insights into key interactions mediated by Bik1 and protein partners. It further offers a basis to rationally perturb +TIP interactions *in vivo* with the aim to understand +TIP network functioning at the systems level.

STAR★METHODS

Detailed methods are provided in the online version of this paper and include the following:

- KEY RESOURCES TABLE
- CONTACT FOR REAGENT AND RESOURCE SHARING
- EXPERIMENTAL MODEL DETAILS
- METHOD DETAILS
  - Protein and Peptide Preparations
  - Circular Dichroism (CD) Spectroscopy
  - Size Exclusion Chromatography Followed by Multi-Angle Light Scattering (SEC-MALS)
  - Isothermal Titration Calorimetry (ITC)
  - X-Ray Data Collection and Structure Determination
  - Measurements of Astral Microtubule Behavior and Bik1-3xGFP Distribution in *S. Cerevisiae* Strains
  - Localization of Kar9 in Bim1 ΔETF or Bik1 K46E *S. Cerevisiae* Strains
- QUANTIFICATION AND STATISTICAL ANALYSIS
- DATA AND SOFTWARE AVAILABILITY

SUPPLEMENTAL INFORMATION

Supplemental Information includes two figures and two tables and can be found with this article online at https://doi.org/10.1016/j.str.2018.03.003.

ACKNOWLEDGMENTS

We are indebted to Alain Blanc for help with mass spectrometry, to Natacha Olieric for support with protein purification, and to Ashwani Sharma for technical assistance at the synchrotron beamlines. The X-ray data were collected at beamline X06DA of the Swiss Light Source (Paul Scherrer Institut, Villigen, Switzerland). This work was supported by a Marie Curie COFUND fellowship (to A.K.), and by grants from the Swiss National Science Foundation (31003A_166608; to M.O.S.) and from SystemsX.ch (RTD-TubeX; to Y.B. and M.O.S.).

AUTHOR CONTRIBUTIONS

M.M.S., A.K., X.C., A.-M.F., Y.B., and M.O.S. designed the research. M.M.S., A.K., X.C., and A.-M.F., performed the research. M.M.S., X.Z., A.-M.F., A.K., Y.B., and M.O.S. analyzed the data. M.M.S. and M.O.S. wrote the paper with input from all authors.

DECLARATION OF INTERESTS

The authors declare no competing interests.

Received: December 20, 2017
Revised: February 9, 2018
Accepted: February 28, 2018
Published: March 22, 2018

Figure 7. Role of the Bik1-Bim1 Interaction *In Vivo*

(A) Spot growth assay of background (Bik1-3xGFP, Spc72-GFP), *bim1Δ*, Bim1 ΔETF, and Bik1 K46E cells grown for 2 days on solid YPD agar at 25°C. Spots are from log-phase growing cell samples that was sequentially diluted 10-fold.

(B) Representative images of wild-type (WT), *bim1Δ*, and Bim1 ΔETF metaphase cells expressing Bik1-3xGFP or Bik1 K46E-3xGFP and Spc72-GFP. Red arrowhead marks aMT plus-end. Scale bars, 2 μm.

(C and D) Quantification of Bik1-3xGFP fluorescence intensity (a.u.) on aMT plus-ends ($n > 250$ cells pooled from three independent clones for each mutant, mean ± SD) or Bik1-3xGFP distribution along aMTs by line scanning ($n > 30$ for each mutant, mean ± SEM, only cells positive with Bik1 K46E-3xGFP signal on plus-ends were used in line scanning analysis) in WT, *bim1Δ*, Bim1 ΔETF, and Bik1 K46E metaphase cells. Statistical significance was calculated using two-tailed Student's t test.

(E and F) Measurements of maximum three-dimensional aMT length and lifetime within the 85.6 s image acquisition window in WT, *bim1Δ*, Bim1 ΔETF, and Bik1 K46E metaphase cells using Bik1-3xGFP and Spc72-GFP as the plus- and minus-end markers, respectively ($n > 250$ cells pooled from three independent clones for each mutant, mean ± SD). Statistical significances for aMT length were calculated using two-tailed Student's t test. Differences among lifetime were demonstrated with cumulative distribution plot and assessed with the Kolmogorov-Smirnov test. For all panels, ****$p > 0.0001$; n.s., not significant (Bik1 K46E not shown because MT length was not measurable).

(G) Kar9 localization and its quantification in metaphase cells bearing the WT, Bik1- K46E, or the Bim1 ΔETF mutations. The mean ± SD of three independent clones was plotted. $n > 235$ cells per strain. Scale bars, 2 μm.

(H) Percentage of aligned spindles in metaphase cells bearing the WT, Bik1 K46E, Bim1 ΔETF, or kar9Δ alleles; same cells were quantified as shown in (B). The mean ± SD of three independent clones was plotted.

(I) Relative positioning of the mitotic spindle within the mother cell (d/L; d is the spindle to bud-neck distance and L is the length of the mother cell). The data of three independent clones is represented as a scattered dot plot, showing the mean value ± SD. Statistical significances for spindle positioning was calculated using two-tailed Student's t test; ****$p > 0.0001$.

See also Table S2.

REFERENCES

Akhmanova, A., and Steinmetz, M.O. (2015). Control of microtubule organization and dynamics: two ends in the limelight. Nat. Rev. Mol. Cell Biol. *16*, 711–726.

Badin-Larçon, A.C., Boscheron, C., Soleilhac, J.M., Piel, M., Mann, C., Denarier, E., Fourest-Lieuvin, A., Lafanechère, L., Bornens, M., and Job, D. (2004). Suppression of nuclear oscillations in *Saccharomyces cerevisiae* expressing Glu tubulin. Proc. Natl. Acad. Sci. USA *101*, 5577–5582.

Bjelić, S., De Groot, C.O., Schärer, M.A., Jaussi, R., Bargsten, K., Salzmann, M., Frey, D., Capitani, G., Kammerer, R.A., and Steinmetz, M.O. (2012). Interaction of mammalian end binding proteins with CAP-Gly domains of CLIP-170 and p150(glued). J. Struct. Biol. *177*, 160–167.

Blake-Hodek, K.A., Cassimeris, L., and Huffaker, T.C. (2010). Regulation of microtubule dynamics by Bim1 and Bik1, the budding yeast members of the EB1 and CLIP-170 families of plus-end tracking proteins. Mol. Biol. Cell *21*, 2013–2023.

Buey, R.M., Sen, I., Kortt, O., Mohan, R., Gfeller, D., Veprintsev, D., Kretzschmar, I., Scheuermann, J., Neri, D., Zoete, V., et al. (2012). Sequence determinants of a microtubule tip localization signal (MtLS). J. Biol. Chem. *287*, 28227–28242.

Carvalho, P., Gupta, M.L., Jr., Hoyt, M.A., and Pellman, D. (2004). Cell cycle control of kinesin-mediated transport of Bik1 (CLIP-170) regulates microtubule stability and dynein activation. Dev. Cell *6*, 815–829.

Caudron, F., Andrieux, A., Job, D., and Boscheron, C. (2008). A new role for kinesin-directed transport of Bik1p (CLIP-170) in *Saccharomyces cerevisiae*. J. Cell Sci. *121*, 1506–1513.

Chen, V.B., Arendall, W.B., 3rd, Headd, J.J., Keedy, D.A., Immormino, R.M., Kapral, G.J., Murray, L.W., Richardson, J.S., and Richardson, D.C. (2010). MolProbity: all-atom structure validation for macromolecular crystallography. Acta Crystallogr. D Biol. Crystallogr. *66*, 12–21.

Cordingley, M.G., Callahan, P.L., Sardana, V.V., Garsky, V.M., and Colonno, R.J. (1990). Substrate requirements of human rhinovirus 3C protease for peptide cleavage in vitro. J. Biol. Chem. *265*, 9062–9065.

Davis, I.W., Murray, L.W., Richardson, J.S., and Richardson, D.C. (2004). MOLPROBITY: structure validation and all-atom contact analysis for nucleic acids and their complexes. Nucleic Acids Res. *32* (Web Server issue), W615–W619.

DeLano, W.L. (2002). The PyMOL Molecular Graphics System (DeLano Scientific).

Duellberg, C., Trokter, M., Jha, R., Sen, I., Steinmetz, M.O., and Surrey, T. (2014). Reconstitution of a hierarchical +TIP interaction network controlling microtubule end tracking of dynein. Nat. Cell Biol. *16*, 804–811.

Emsley, P., Lohkamp, B., Scott, W.G., and Cowtan, K. (2010). Features and development of coot. Acta Crystallogr. D Biol. Crystallogr. *66*, 486–501.

Honnappa, S., Okhrimenko, O., Jaussi, R., Jawhari, H., Jelesarov, I., Winkler, F.K., and Steinmetz, M.O. (2006). Key interaction modes of dynamic +TIP networks. Mol. Cell *23*, 663–671.

Honnappa, S., Gouveia, S.M., Weisbrich, A., Damberger, F.F., Bhavesh, N.S., Jawhari, H., Grigoriev, I., van Rijssel, F.J., Buey, R.M., Lawera, A., et al. (2009). An EB1-binding motif acts as a microtubule tip localization signal. Cell *138*, 366–376.

Howard, J., and Hyman, A.A. (2003). Dynamics and mechanics of the microtubule plus end. Nature *422*, 753–758.

Hüls, D., Storchova, Z., and Niessing, D. (2012). Post-translational modifications regulate assembly of early spindle orientation complex in yeast. J. Biol. Chem. *287*, 16238–16245.

Kabsch, W. (2010). XDS. Acta Crystallogr. D Biol. Crystallogr. *66*, 125–132.

Knop, M., Siegers, K., Pereira, G., Zachariae, W., Winsor, B., Nasmyth, K., and Schiebel, E. (1999). Epitope tagging of yeast genes using a PCR-based strategy: more tags and improved practical routines. Yeast *15*, 963–972.

Kumar, A., Manatschal, C., Rai, A., Grigoriev, I., Degen, M.S., Jaussi, R., Kretzschmar, I., Prota, A.E., Volkmer, R., Kammerer, R.A., et al. (2017). Short linear sequence motif LxxPTPh targets diverse proteins to growing microtubule ends. Structure *25*, 924–932.

Karplus, P.A., and Diederichs, K. (2012). Linking crystallographic model and data quality. Science *336*, 1030–1033.

Krull, A., Steinborn, A., Ananthanarayanan, V., Ramunno-Johnson, D., Petersohn, U., and Tolić-Nørrelykke, I.M. (2014). A divide and conquer strategy for the maximum likelihood localization of low intensity objects. Opt. Express *22*, 210–228.

Laughery, M.F., Hunter, T., Brown, A., Hoopes, J., Ostbye, T., Shumaker, T., and Wyrick, J.J. (2015). New vectors for simple and streamlined CRISPR-Cas9 genome editing in *Saccharomyces cerevisiae*. Yeast *32*, 711–720.

Manatschal, C., Farcas, A.M., Degen, M.S., Bayer, M., Kumar, A., Landgraf, C., Volkmer, R., Barral, Y., and Steinmetz, M.O. (2016). Molecular basis of Kar9-Bim1 complex function during mating and spindle positioning. Mol. Biol. Cell *27*, 3729–3745.

Matsuo, Y., Maurer, S.P., Yukawa, M., Zakian, S., Singleton, M.R., Surrey, T., and Toda, T. (2016). An unconventional interaction between Dis1/TOG and Mal3/EB1 in fission yeast promotes the fidelity of chromosome segregation. J. Cell Sci. *129*, 4592–4606.

Maurer, S.P., Cade, N.I., Bohner, G., Gustafsson, N., Boutant, E., and Surrey, T. (2014). EB1 accelerates two conformational transitions important for microtubule maturation and dynamics. Curr. Biol. *24*, 372–384.

McCoy, A.J., Grosse-Kunstleve, R.W., Adams, P.D., Winn, M.D., Storoni, L.C., and Read, R.J. (2007). Phaser crystallographic software. J. Appl. Crystallogr. *40*, 658–674.

Miller, R.K., and Rose, M.D. (1998). Kar9p is a novel cortical protein required for cytoplasmic microtubule orientation in yeast. J. Cell Biol. *140*, 377–390.

Miller, R.K., D'Silva, S., Moore, J.K., and Goodson, H.V. (2006). The CLIP-170 orthologue Bik1p and positioning the mitotic spindle in yeast. Curr. Top. Dev. Biol. *76*, 49–87.

Mishima, M., Maesaki, R., Kasa, M., Watanabe, T., Fukata, M., Kaibuchi, K., and Hakoshima, T. (2007). Structural basis for tubulin recognition by cytoplasmic linker protein 170 and its autoinhibition. Proc. Natl. Acad. Sci. USA *104*, 10346–10351.

Moore, J.K., D'Silva, S., and Miller, R.K. (2006). The CLIP-170 homologue Bik1p promotes the phosphorylation and asymmetric localization of Kar9p. Mol. Biol. Cell *17*, 178–191.

Moore, J.K., and Miller, R.K. (2007). The cyclin-dependent kinase Cdc28p regulates multiple aspects of Kar9p function in yeast. Mol. Biol. Cell *18*, 1187–1202.

Olieric, N., Kuchen, M., Wagen, S., Sauter, M., Crone, S., Edmondson, S., Frey, D., Ostermeier, C., Steinmetz, M.O., and Jaussi, R. (2010). Automated seamless DNA co-transformation cloning with direct expression vectors applying positive or negative insert selection. BMC Biotechnol. *10*, 56.

Podolski, M., Mahamdeh, M., and Howard, J. (2014). Stu2, the budding yeast XMAP215/Dis1 homolog, promotes assembly of yeast microtubules by increasing growth rate and decreasing catastrophe frequency. J. Biol. Chem. *289*, 28087–28093.

Roberts, A.J., Goodman, B.S., and Reck-Peterson, S.L. (2014). Reconstitution of dynein transport to the microtubule plus end by kinesin. Elife *3*, e02641.

Sauter, N.K., Grosse-Kunstleve, R.W., and Adams, P.D. (2004). Robust indexing for automatic data collection. J. Appl. Crystallogr. *37*, 399–409.

Schneider, C.A., Rasband, W.S., and Eliceiri, K.W. (2012). NIH Image to ImageJ: 25 years of image analysis. Nat. Methods *9*, 671–675.

Slep, K.C. (2010). Structural and mechanistic insights into microtubule end-binding proteins. Curr. Opin. Cell Biol. *22*, 88–95.

Steinmetz, M.O., and Akhmanova, A. (2008). Capturing protein tails by CAP-Gly domains. Trends Biochem. Sci. *33*, 535–545.

van der Vaart, B., Manatschal, C., Grigoriev, I., Olieric, V., Gouveia, S.M., Bjelic, S., Demmers, J., Vorobjev, I., Hoogenraad, C.C., Steinmetz, M.O., and Akhmanova, A. (2011). SLAIN2 links microtubule plus end-tracking proteins and controls microtubule growth in interphase. J. Cell Biol. *193*, 1083–1099.

van der Vaart, B., Fischböck, J., Mieck, C., Pichler, P., Mechtler, K., Medema, R.H., and Westermann, S. (2017). TORC1 signaling exerts spatial control over microtubule dynamics by promoting nuclear export of Stu2. J. Cell Biol. *216*, 3471–3484.

Vagin, A.A., Steiner, R.A., Lebedev, A.A., Potterton, L., McNicholas, S., Long, F., and Murshudov, G.N. (2004). REFMAC5 dictionary: organization of prior chemical knowledge and guidelines for its use. Acta Crystallogr. D Biol. Crystallogr. *60*, 2184–2195.

Weisbrich, A., Honnappa, S., Jaussi, R., Okhrimenko, O., Frey, D., Jelesarov, I., Akhmanova, A., and Steinmetz, M.O. (2007). Structure-function relationship of CAP-Gly domains. Nat. Struct. Mol. Biol. *14*, 959–967.

Wolyniak, M.J., Blake-Hodek, K., Kosco, K., Hwang, E., You, L., and Huffaker, T.C. (2006). The regulation of microtubule dynamics in *Saccharomyces cerevisiae* by three interacting plus-end tracking proteins. Mol. Biol. Cell *17*, 2789–2798.

STAR★METHODS

KEY RESOURCES TABLE

REAGENT or RESOURCE	SOURCE	IDENTIFIER
Bacterial and Virus Strains		
BL21(DE3)	Novagen	Prod: #69450-3
Mach1	Thermo Fischer	Prod: #C862003
Chemicals, Peptides, and Recombinant Proteins		
ETF peptide (peptide sequences are specified in the methods)	This paper	N/A
ETY peptide	This paper	N/A
LxxPTPh peptide	Kumar et al., 2017	N/A
PreScission protease	produced in-house	N/A
Sodium cacodylate trihydrate	Hampton Research	HR2-241
SxIP peptide	Buey et al., 2012	N/A
TCEP	Sigma-Aldrich	646547
Deposited Data		
Crystal structure of Bik1CG	This paper	PDB: 6FC5
Crystal structure of Bik1CG-ETF complex	This paper	PDB: 6FC6
Experimental Models: Organisms/Strains		
All *S. cerevisiae* strains used in this study are listed in Table S2	This paper	N/A
Oligonucleotides for CRISPR		
Bim1-ΔETF guide RNA 5'-CAACAACTTGAT CATCGACGAGG-3'	This paper	N/A
Bim1-ΔETF_F 5'-GGTGAGGTTGGCGTGAG CAACAACTTGATCATCGACGAGTAAGTTG AGAACTAAAAAGCAGTATTGTTTTCGAA TATGT-3'	This paper	N/A
Bim1-ΔETF_R 5'-ACATATTCGAAAACAATA CTGCTTTTTAGTTCTCAACTTACTCGTCG ATGATCAAGTTGTTGCTCACGCCAACC TCACC-3'	This paper	N/A
Bik1_gRNA_125bp_O1 5'-GATCTCCATCG TTCTTACCAATGTGTTTTAGAGCTAG-3'	This paper	N/A
Bik1_K46E-F (template) 5'-GCTGGAATGTTT GCTGGTGTAGACTTACTTGCCAACATTGGT GAGAACGATGGATCATTCATGGGGAAGAA GTATTTTCAAACGGAGTATCCTC-3'	This paper	N/A
Bik1_K46E-R (template) 5'-GAGGATACTCC GTTTGAAAATACTTCTTCCCCATGAATGAT CCATCGTTCTCACCAATGTTGGCAAGTAA GTCTACACCAGCAAACATTCCAGC-3'	This paper	N/A
Recombinant DNA		
Plasmid: Bik1CG (aa 1-100) in PSTcm9	This paper	N/A
Plasmid: Bik1CG K46E (aa 1-100) in PSTcm9	This paper	N/A
Plasmid: Bik1cc (aa 182-396) in PSTcm2	This paper	N/A
Plasmid: Bim1C (aa 194-344)	Manatschal et al., 2016	N/A
Plasmid: Bik1C ΔETF (aa 194-341) in PSTcm2	This paper	N/A
Plasmid: Stu2Ctail (aa 855-888) in PSTcm9	This paper	N/A

(*Continued on next page*)

Continued

REAGENT or RESOURCE	SOURCE	IDENTIFIER
Software and Algorithms		
ASTRA	Wyatt Technolgies	https://www.wyatt.com/products/software/astra.html
Coot	Emsley et al., 2010	http://www.ccp4.ac.uk
Chirascan	Applied Photophysics	http://www.photophysics.com/
ImageJ	Schneider et al., 2012	https://fiji.sc/
MolProbity	Chen et al., 2010	http://molprobity.biochem.duke.edu
Origin	OriginLab	https://www.originlab.com
PHASER	McCoy et al., 2007	http://www.ccp4.ac.uk
PHENIX	https://www.phenix-online.org/	https://www.phenix-online.org/
Pymol	Schrödinger, LLC	http://www.pymol.org
REFMAC5	Vagin et al., 2004	http://www.ccp4.ac.uk
VisiVIEW	Visitron Systems	http://www.visitron.de
XDS	Kabsch, 2010	http://xds.mpimf-heidelberg.mpg.de/
Other		
Agilent UltiMate3000 HPLC (full MALS setup in methods)	Agilent	N/A
HisTrap FF 5ml	GE Healthcare	Prod: #17531901
HiLoad 16/60 Superdex 75 pg column	GE Healthcare	Prod: #28989333
HiLoad 16/60 Superdex 200 pg column	GE Healthcare	Prod: #28989335
MicroCal ITC200 Isothermal Titration Calorimeter	MicroCal	N/A
Superdex 200 Increase 10/300 GL	GE Healthcare	Prod: #28990944

CONTACT FOR REAGENT AND RESOURCE SHARING

Further information and requests for resources and reagents should be directed to and will be fulfilled by the Lead Contact, Michel Steinmetz (michel.steinmetz@psi.ch)

EXPERIMENTAL MODEL DETAILS

In this study, all yeast strains (*S. cerevisiae*) were derived from the S288C background. Expression of recombinant proteins for *in vitro* studies were produced in the E. coli strain BL21(DE3).

METHOD DETAILS

Protein and Peptide Preparations

The DNA encoding the CAP-Gly domain of *S. cerevisiae* Bik1 (Bik1CG, residues 1-100; Uniprot ID: P11709) and the C-terminal part of *S. cerevisiae* Stu2 (Stu2Ctail, residues 855-888; Uniprot ID: P46675) were cloned into the pET-based bacterial expression vector PSTCm9, which encodes for an N-terminal thioredoxin, a 6x His-tag and a PreScission cleavage site using a positive selection method (Olieric et al., 2010). The coiled-coil domain of Bik1 (Bik1cc, residues 182-396; Uniprot ID: Q80VC9) was cloned into the PSTCm2 vector that encodes for an N-terminal 6x His-tag and a PreScission cleavage site (Olieric et al., 2010). The bacterial expression vector for the C-terminal domain of *S. cerevisiae* Bim1 (Bim1C, residues 194-344; Uniprot ID: P40013) has been reported previously (Manatschal et al., 2016). This plasmid was utilized to generate the Bim1C construct that lacked the C-terminal ETF motif of Bim1 (denoted Bim1C ΔETF, residues 194-341) by applying a standard PCR approach and cloning into the PSTCm2 vector. The mutant Bik1CG K46E clone was obtained by standard PCR-based site-directed mutagenesis.

Protein production was performed in the *E. coli* strain BL21(DE3) (Stratagene) in LB media containing 50 μg/ml of kanamycin. When the cultures had reached an OD_{600} of 0.6 at 37°C, they were cooled down to 20°C, induced with 1 mM isopropyl 1-thio-β-D-galactopyranoside (IPTG) and shaken for another 16 hours at 20°C. After harvesting and washing of the cells with Dulbecco PBS buffer (Millipore), the cells were sonicated in the presence of the protease inhibitor cOmplete cocktail (Roche) in lysis buffer (50 mM HEPES, pH 8, supplemented with 500 mM NaCl, 10 mM imidazole, 2 mM β-mercaptoethanol, 0.1% bovine deoxyribonuclease I).

Proteins were purified by immobilized metal-affinity chromatography (IMAC) on a HisTrap HP Ni^{2+}-Sepharose column (GE Healthcare) at 4°C following the instructions of the manufacturer. The column was equilibrated in IMAC buffer A (50 mM HEPES, pH 8,

supplemented with 500 mM NaCl, 10 mM imidazole, 2 mM β-mercaptoethanol). Proteins were eluted by IMAC buffer B (IMAC buffer A containing 400 mM imidazole in total). In the case of Bik1CG, Bik1CG K46E or Bik1cc, the N-terminal fusion proteins and tags were cleaved off by an in-house produced HRV 3C protease (Cordingley et al., 1990) in IMAC buffer A for 16 hours at 4°C. The cleaved samples were reapplied on the IMAC column to separate cleaved from uncleaved protein.

Protein samples were concentrated and loaded onto a size exclusion chromatography (SEC) HiLoad Superdex 75 16/60 column (GE Healthcare), which was equilibrated in SEC buffer (20 mM Tris-HCl, pH 7.5, supplemented with 500 mM NaCl and 1 mM DTT). In the case of Bim1C, Stu2C and Bik1cc, the SEC buffer contained 150 mM NaCl. The fractions of the respective main peaks were pooled and concentrated to 10 mg/ml. Protein quality and identity were assessed by SDS-PAGE and mass spectrometry, respectively.

The ETF (residues 334-344 of *S. cerevisiae* Bim1), the ETY (F344 mutated to Y), SxIP (KPSKIPTLQRKSW, a derivative of MACFp1; Buey et al., 2012) and LxxPTPh (residues 615-633 of *S. cerevisiae* Kar9, Uniprot ID: P32526; Manatschal et al., 2016) peptides were produced by standard peptide chemistry. Peptide quality and identity were assessed by high performance liquid chromatography and mass spectrometry, respectively. Peptides were dissolved in PBS buffer pH 7.4 (137 mM NaCl, 2.7 mM KCl, 10 mM Na_2HPO_4 and 1.8 mM KH_2PO_4) at a typical concentration of 10 mM.

Circular Dichroism (CD) Spectroscopy

The CD spectrum of Bik1cc (0.25 mg/ml in PBS) was recorded at 5°C on a Chirascan-Plus spectrophotometer (Applied Photophysics Ltd.) equipped with a computer-controlled Peltier element using a quartz cuvette of 1 mm optical path length. Thermal unfolding profiles were recorded by CD at 222 nm by continuous heating at 1°C min^{-1}. The apparent midpoint of the transition, T_m, was determined by fitting of the data points using the R nonlinear least square fitting function based on a sigmoid model.

Size Exclusion Chromatography Followed by Multi-Angle Light Scattering (SEC-MALS)

For the SEC-MALS experiment at 25°C, a Superdex 10/30 column (GE Healthcare) was equilibrated in 20 mM Tris-HCl, pH 7.5, supplemented with 150 mM NaCl and 1 mM DTT (SEC buffer) at a flow rate of 0.5 ml/min on an Agilent UltiMate3000 HPLC. 30 μl of Bik1CG or Bik1cc protein solutions at 5 mg/ml were injected onto the column and the mass was determined using the miniDAWN TREOS and Optilab T-rEX refractive index detectors (Wyatt Technology). The Zimm model was chosen for data fitting, which was performed in the ASTRA 6 software.

Isothermal Titration Calorimetry (ITC)

All proteins and peptide samples were buffer-exchanged to ITC buffer (PBS buffer supplemented with 0.5 mM TCEP). ITC experiments were performed either at 20°C (experiments with Stu2-C) or 25°C (all other experiments) on an iTC 200 machine (MicroCal) using 15 injections of 2.6 μl. 50-100 μM of Bim1C, Bik1cc, Bim1C ΔETF, Bim1C-MACF SxIP or Bim1C-Kar9 LxxPTPh were loaded into the sample cell. 500-1000 μM Bik1CG, Bim1C ETF, Stu2C, MACF SxIP, Kar9 LxxPTPh or Bik1CG K46E were loaded into the syringe. In the case of Bik1 CG:Bim1 ETF, Bik1CG was present in the cell (50 μM) and Bim1 ETF in the syringe (500 μM). Fits of the binding isotherms were obtained by using a nonlinear least squares minimization method. The one set of site model provided in the software package of the calorimeter was utilized to determine the equilibrium dissociation constant, K_d. In most cases where a binding reaction took place, two independent experiments were performed. The determined K_d values are reported in Table S1. The K_d value of "Exp1" in Table S1 is reported in the main text. Standard errors were derived from the nonlinear least square fitting of the respective binding isotherms.

X-Ray Data Collection and Structure Determination

Bik1CG was concentrated to 20 mg/ml and DTT to a final concentration of 5 mM was added to the sample. The screening of crystallization conditions was performed using a Mosquito robot (TTP Labtech) in 96 well plates using the vapor diffusion hanging drop method at 20°C. Crystals appeared overnight in drops of a 1:1 (200 nl each) mixture of Bik1CG and mother liquor (0.1 M sodium cacodylate, pH 6.5, 1.0 M sodium citrate) The crystals were cryo-protected by transferring them into mother liquor supplemented with 25% glycerol and were flash frozen in liquid nitrogen.

In order to co-crystallize Bik1CG with the Bim1C ETF peptide, Bik1CG was mixed with Bim1C ETF that was also dissolved in the Bik1CG SEC buffer. The final concentration of the complex was 10 mg/ml and 5 mM DTT was added. Crystals were obtained at 0.1 M sodium cacodylate, pH 6.4, 1.0 M sodium citrate. The crystals were cryo-protected by transferring them into mother liquor supplemented with 25% glycerol and were flash frozen in liquid nitrogen.

X-ray diffraction data of Bik1 CG crystals were collected at the X06DA macromolecular crystallography beamline at the Swiss Light Source (Paul Scherrer Institut) at a wavelength of 1 Å. The data were indexed with LABELIT (Sauter et al., 2004), and refined and integrated with XDS (Kabsch, 2010). The Bik1CG structure was solved by molecular replacement with PHASER (McCoy et al., 2007) using the structure of the CAP-Gly domain of the p150glued structure (PDB ID 2HKN) as a search model. The Bik1CG structure was subsequently used to solve the structure of the Bik1CG-Bim1-ETF complex by molecular replacement. Several rounds of manual model building in COOT (Emsley et al., 2010) and refinement in REFMAC (Vagin et al., 2004). Both the Bik1CG and Bik1CG-Bim1C ETF structures were validated by MolProbity. Figures were prepared using PyMOL (DeLano, 2002). Data collection and refinement statistics are given in Table 1.

Measurements of Astral Microtubule Behavior and Bik1-3xGFP Distribution in *S. Cerevisiae* Strains

All yeast strains used in this study were derived from the S288C background. Yeast cells expressing the microtubule plus-end marker Bik1-3xGFP and SPB marker Spc72-GFP from endogenous loci were grown and imaged in synthetic complete (SC) medium at 25°C, except that at 30°C for aMT dynamics. Deletion of BIM1 and BIK1 was performed as described (Knop et al., 1999), the Bim1 ΔETF mutants and the point mutation Bik1 K46E were created with the CRISPR-cas9 system (Laughery et al., 2015) and sequenced to validate.

Time-lapse movies were acquired using a back-illuminated EM-CCD camera Evolve 512(Photometrics, Inc.) mounted on a spinning disk microscope with a motorized piezo stage (ASI MS-2000) and 100x 1.46 NA alpha Plan Apochromat oil immersion objective, driven by Metamorph based software VisiVIEW (Visitron Systems). 17 Z-section images separated by 0.24μm increments were captured every 1.07 sec for 85.6 sec. To determine the length of astral microtubules, three-dimensional coordinates of microtubule plus-end and the corresponding SPB were extracted with the Low Light Tracking Tool (Krull et al., 2014) and the distance between the plus-end and the SPB represents the length of a microtubule. The maximum length and lifetime of each microtubule within the recorded window were then recorded. For line scan analysis, sum slices projections of Z stacks were used, a 5px (666.7 nm) width line was used to scan aMTs from plus-ends toward SPBs. To quantify the fluorescence intensity of Bik1-3xGFP on plus-ends, a region of interest (ROI) was drawn around the area of interest (AOI) and the integrated density was quantified. An identically sized ROI was put next to the AOI to determine the background signal. The background intensity was subtracted from the ROI intensity to yield the fluorescent intensity (a.u.).

Localization of Kar9 in Bim1 ΔETF or Bik1 K46E *S. Cerevisiae* Strains

Specific Bik1 and Bim1 mutations were introduced at the endogenous locus via the CRISPR/Cas9 gene editing methodology (Laughery et al., 2015). The integration was confirmed by PCR and sequencing. The Kar9 protein was tagged at the endogenous locus with 3xsfGFP:KanMX cassette, while the CFP-Tub1 construct was inserted at the TRP1 locus using the integrative plasmid pRS304.

Yeast strains were exponentially grown in synthetic media lacking tryptophan. Cells were harvested by centrifugation at 600 x g for 2 minutes and taken onto microscopy slides. Strains were imaged on a Personal Delta Vision microscope, with z stacks of 11 layers (step size of 0.3 μm). Images were analyzed with Fiji (ImageJ) using sum projections.

All yeast strains generated in this study are summarized in Table S2.

QUANTIFICATION AND STATISTICAL ANALYSIS

In case of ITC, the standard errors were derived from the nonlinear least square fits of the respective binding isotherms. For the *in vivo* experiments in yeast, the statistical significance was calculated by applying the two-tailed student t-test.

DATA AND SOFTWARE AVAILABILITY

Atomic coordinates and structure factors for Bik1CG and Bik1CG-ETF have been deposited in the RCSB Protein Data Bank (PDB) under accession numbers 6FC5 and 6FC6.

Structure, Volume *26*

Supplemental Information

Structure-Function Relationship of the Bik1-Bim1 Complex

Marcel M. Stangier, Anil Kumar, Xiuzhen Chen, Ana-Maria Farcas, Yves Barral, and Michel O. Steinmetz

Table S1

Table S1, related to Figure 1, 5 and 6. K_d Values determined by ITC.
Various experiments were repeated to confirm the K_d values.

Cell	Syringe	$K_{d\ Exp1}$ [µM]	$K_{d\ Exp2}$ [µM]
Bim1C	Bik1CG	1.2 ± 0.3	1.0 ± 0.3
Bik1CG	ETF	5.6 ± 0.8	4.7 ± 0.6
Bim1C ΔETF	Bik1CG	n.b.	-
Bim1C	Bik1CG K46E	n.b.	-
Bik1cc	Stu2Ctail	0.6 ± 0.1	0.8 ± 0.1
Bim1C	Stu2Ctail	n.b.	-
Bim1C	SxIP	11.6 ± 0.2	n.d. [a]
Bim1C-Bik1CG	SxIP	13.0 ± 0.6	n.d.
Bim1C-SxIP	Bik1CG	2.0 ± 0.6	n.d.
Bim1C	LxxPTPh	2.2 ± 0.6	2.2 ± 0.5
Bim1C-Bik1CG	LxxPTPh	2.7 ± 0.5	n.d.

n.b., no binding; n.d., not determined

[a] A K_d value of 13.8 µM for this interaction is reported in (Kumar et al., 2017) using ITC.

± refers to the standard error of the least square fit (i.e., assuming a one set of site model) versus the data points.

Table S2

Table S2, related to Figure 7. Summary of the yeast strains that has been used in this study.

Yeast strain number (yYB)	Mating type	Genotype	Source
11069, 11070	a	Bik1-3xGFP::hphNT1 Spc72-GFP::HIS ura3-52 his3Δ200 leu2 lys2-801 trp1Δ63 Ade2+	This study
11068	alpha	Bik1-3xGFP::hphNT1 Spc72-GFP::HIS ura3-52 his3Δ200 leu2 lys2-801 trp1Δ63 Ade2+	This study
11077, 11078, 11079	a	Bik1-3xGFP::hphNT1 Spc72-GFP::HIS bim1::hphNT1 ura3-52 his3Δ200 leu2 lys2-801 trp1Δ63 Ade2+	This study
13751, 13752, 13753	a	Bik1-3xGFP::hphNT1 Spc72-GFP::HIS Bim1-ΔETF ura3-52 his3Δ200 leu2 lys2-801 trp1Δ63 Ade2+	This study
14945, 14946, 14947	alpha	Bik1-K46E-3xGFP::hphNT1 Spc72-GFP::HIS ura3-52 his3Δ200 leu2 lys2-801 trp1Δ63 Ade2+	This study
11263	a	bik1::NatMX Spc72-GFP::HIS ura3-52 his3Δ200 leu2 lys2-801 trp1Δ63 Ade2+	This study
8597, 8600, 8602	a	CFP-Tub1:Trp1 kar9::His3 ura3-52 leu2 lys2-801 Ade2+	Manatschal et al., 2016
8461, 8462, 8463	a	CFP-Tub1:Trp1 kar9::Kar9-wt-3xGFP:KanMX ura3-52 his3Δ200 leu2 lys2-801 ade2-101	Manatschal et al., 2016
12656, 12657	a	CFP-Tub1:Trp1 kar9::Kar9-wt-3xsfGFP:KanMX ura3-52 his3Δ200 leu2 lys2-801 Ade2+	Manatschal et al., 2016
14940, 14941	a	CFP-Tub1:Trp1 kar9::Kar9-wt-3xsfGFP:KanMX Bik1-K46E ura3-52 his3Δ200 leu2 lys2-801 Ade2+	This study
14942	alpha	CFP-Tub1:Trp1 kar9::Kar9-wt-3xsfGFP:KanMX Bik1-K46E ura3-52 his3Δ200 leu2 lys2-801 Ade2+	This study
14491, 14831	a	CFP-Tub1::Trp1 kar9::Kar9-wt-3xsfGFP:KanMX Bim1-ΔETF ura3-52 his3Δ200 leu2 lys2-801 Ade2+	This study
14492, 14830	alpha	CFP-Tub1::Trp1 kar9::Kar9-wt-3xsfGFP:KanMX Bim1-ΔETF ura3-52 his3Δ200 leu2 lys2-801 Ade2+	This study

Figure S1

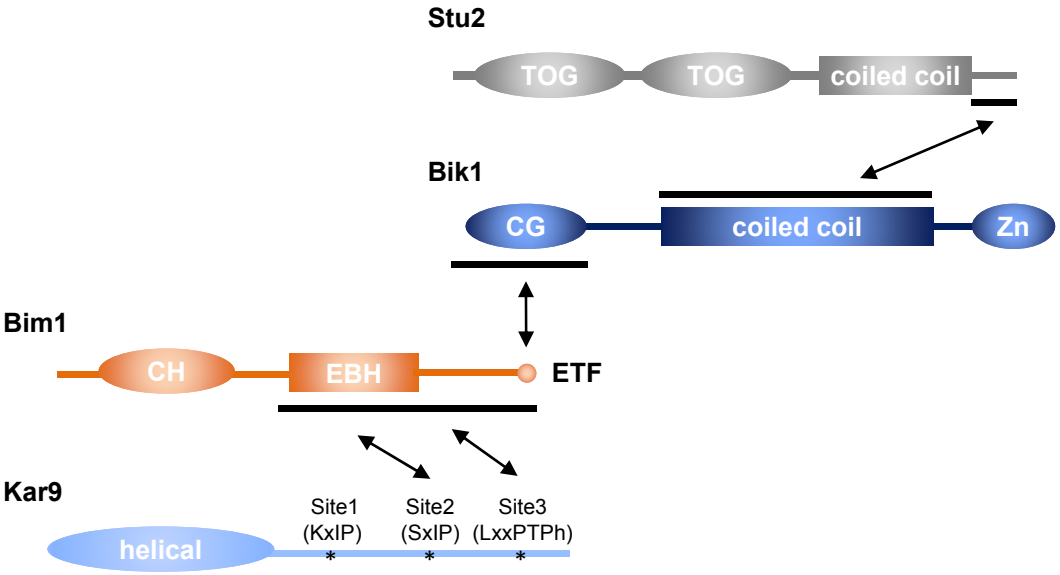

Figure S1, related to Figures 1, 5 and 6. Schematic representation of +TIP network formed between Bik1, Stu2, Bim1 and Kar9.

The interactions highlighted by double arrows are reported in (Wolyniak et al., 2006; Blake-Hodek et al., 2010; Manatschal et al., 2016). Note that not in all instances it is clear whether the interactions are direct or indirect; see also Introduction. The protein fragments and domains reporting the interactions are indicated by horizontal black lines.

Figure S2

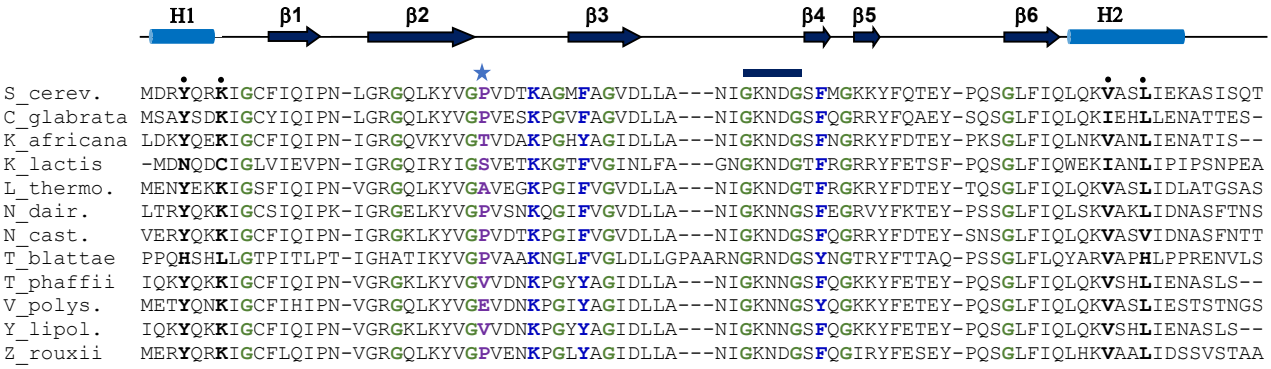

Figure S2, related to Figure 2. Multiple sequence alignment of budding yeast Bik1 CAP-Gly domains.

The characteristic glycine residues and GKNDG motif of CAP-Gly domains are indicated in green and with a black horizontal bar on top of the alignment, respectively. The position of the β2-β3 loop residue that in the case of p150CG interacts with the EBH domain of EB1 (Ala49; Honnappa et al., 2006) is highlighted with an asterisk and the corresponding residues are shown in bold and in purple. Key residues of the exposed hydrophobic cavity of CAP-Gly are shown in bold and dark blue. Conserved residues in both the N- and C-terminal helices are highlighted in bold and with a dot on the top of the alignment.